Spreading and leveling of finite thin films with elastic interfaces: An eigenfunction expansion approach

N C Papanicolaou[1] **and I C Christov**[2]

[1] Department of Computer Science, University of Nicosia, 46 Makedonitissas Avenue, CY-2417 Nicosia, Cyprus

[2] School of Mechanical Engineering, Purdue University, West Lafayette, Indiana 47907, USA

E-mail: papanicolaou.n@unic.ac.cy,christov@purdue.edu

Abstract. The flow of a thin viscous liquid layer under an elastic film arises in natural processes, such as magmatic intrusions between rock strata, and industrial applications, such as coating surfaces with cured polymeric films. We study the linear dynamics of small perturbations to the equilibrium state of the film in a closed trough (finite film). Specifically, we are interested in the spreading (early-time) and leveling (late-time) dynamics as the film adjusts to equilibrium, starting from different initial perturbations. We consider both smooth and non-smooth spatially symmetric and localized initial conditions (perturbations). We find the exact series solutions for the film height, using the sixth-order complete orthonormal eigenfunctions associated with the posed initial-boundary-value problem derived in our previous work [Papanicolaou N C and Christov I C 2023 *J. Phys.: Conf. Ser.* **2675** 012016]. We show that the evolution of the perturbations begins with the spreading of the localized perturbations, followed by their mutual interaction as they spread, and finally, interactions with the confining lateral boundaries of the domain as the perturbations level. In particular, we highlight how the leading eigenvalues of the problem determine the scalings of certain figures of merit with time.

1. Introduction

The flow of a thin viscous liquid layer under an elastic film [1, 2] arises in natural processes, such as magmatic intrusions between rock strata [3, 4, 5], and industrial applications, such as coating of surfaces with cured polymeric films [6, 7], growth of epitaxial films for optoelectronics [8] and semiconductors [9], microfluidic actuators [10], impact mitigation [11, 12], and adhesion [13, 14], to name a few. In our previous work [15], we considered the linear dynamics of a *finite* thin film with an elastic interface. Specifically, we derived the set of complete sixth-order orthonormal eigenfunctions associated with the initial boundary value problem. In this work, we continue our studies of the linear dynamics of small perturbations to the equilibrium state of the film in a closed trough (finite film).

Specifically, we are interested in the spreading (early time) and leveling (late time) dynamics as the film adjusts to equilibrium, starting from different initial perturbations. The motivation for the present study is the recent work of Sæter et al. [16], who performed a combined experimental-numerical study of the fate of localized *blisters* [17] on the surface of a laterally unbounded elastic-plated film. They focused on the nonlinear regime of coalescence and its self-similar dynamics, noting an "anomalous exponential growth with time, contrasting the power-law solutions usually describing the self-similar behavior of lubrication flows" (e.g., [18, 19]).

To further understand this behavior, we analyze the *linear* dynamics of blisters on the elastic surface of an *confined* thin film, the governing equations of which are reviewed in section 2. Using the complete

sixth-order orthonormal eigenfunctions from our previous work [15], which are reviewed in section 3, we find the exact series solution for the film height by separation of variables in section 4. Next, in section 5, we consider non-smooth (section 5.1) and smooth (section 5.2) forms of the spatially symmetric initial conditions representing the localized perturbations that create blisters on the surface of the film. We show that the evolution of the perturbations begins with the spreading of the localized perturbations, followed by their mutual interaction as they spread, and finally, interactions with the finite lateral boundaries of the domain as the perturbations level. In particular, we highlight the exponential decay in time of various relevant quantities, whose time scales are set by the leading eigenvalues of the problem. Conclusions are stated in section 6.

2. Governing equations

Using lubrication theory (i.e., a long-wave approximation) [20, 21, 22], it can be shown [1, 23, 15] that a slender, elastic-plated film's height $h(x,t)$ obeys the sixth-order *thin-film equation*

$$\frac{\partial h}{\partial t} = \frac{\partial}{\partial x}\left\{\frac{h^3}{12\mu_f}\left[\rho_f g\frac{\partial h}{\partial x} + B\frac{\partial^5 h}{\partial x^5}\right]\right\}, \tag{2.1}$$

where μ_f is the (Newtonian) fluid's dynamic viscosity, ρ_f is its density, and B is the elastic interface's bending rigidity. The equilibrium film height is h_0, the trough has an axial length $2\ell \gg h_0$, and the acceleration due to gravity is denoted by g. A schematic is shown in figure 1.

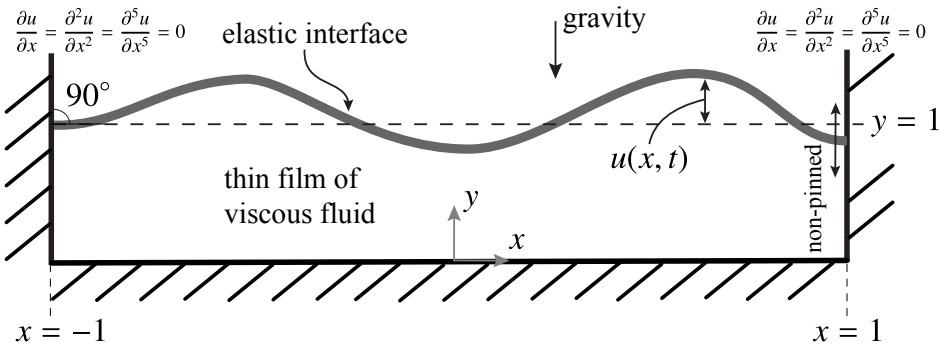

Figure 1. Schematic of a finite thin film with an elastic interface in terms of the dimensionless variables of the problem. The perturbation of the flat state is denoted $u(x,t)$. The domain and boundary conditions on u at $x = \pm 1$ (non-pinned, 90° contact angle, and no flux through the vertical confining walls) are indicated.

Making the problem dimensionless through the transformations $x \mapsto \ell x$, $h \mapsto h_0 h$, $t \mapsto t_c t$ and choosing $t_c = 12\mu_f \ell^6 / B h_0^3$ to be the so-called "viscous-elastic" timescale [24], (2.1) becomes

$$\frac{\partial h}{\partial t} = \frac{\partial}{\partial x}\left[h^3\left(\mathrm{Bo}\frac{\partial h}{\partial x} + \frac{\partial^5 h}{\partial x^5}\right)\right], \tag{2.2}$$

where the *Bond number*

$$\mathrm{Bo} = \frac{\rho_f g \ell^4}{B} \tag{2.3}$$

quantifies the effect of gravity relative to the bending resistance.

As in [15, 19], we are interested in *small perturbations* to the flat state: $h(x,t) = 1 + u(x,t)$, where $\max_{x,t}|u| \ll 1$. Then, to leading-order in u, (2.2) becomes

$$\frac{\partial u}{\partial t} = \mathrm{Bo}\frac{\partial^2 u}{\partial x^2} + \frac{\partial^6 u}{\partial x^6}, \tag{2.4}$$

which is a linear sixth-order partial differential equation of "parabolic" type [19]. As discussed in [15, 19], for a free (non-pinned) film in a closed trough, as shown in figure 1, the boundary conditions for (2.4) are

$$\frac{\partial u}{\partial x} = \frac{\partial^2 u}{\partial x^2} = \frac{\partial^5 u}{\partial x^5} = 0 \quad \text{at} \quad x = \pm 1. \tag{2.5}$$

Here, we consider the simplest form of (2.4), which occurs when Bo = 0 (i.e., gravity is negligible).

3. The complete orthonormal set of sixth-order eigenfunctions

Based on the above discussion, consider the following sixth-order initial boundary value problem (IBVP) for $u = u(x, t)$:

$$\begin{cases} \dfrac{\partial u}{\partial t} - \dfrac{\partial^6 u}{\partial x^6} = 0, & (x,t) \in (-1,1) \times \in (0,\infty), & \text{(3.1a)} \\ \left.\dfrac{\partial u}{\partial x}\right|_{x=\pm 1} = \left.\dfrac{\partial^2 u}{\partial x^2}\right|_{x=\pm 1} = \left.\dfrac{\partial^5 u}{\partial x^5}\right|_{x=\pm 1} = 0, & t \in (0,\infty), & \text{(3.1b)} \\ u(x,0) = u^0(x), & x \in (-1,1), & \text{(3.1c)} \end{cases}$$

for a given $u^0 \in L^2[-1,1]$.

To solve IBVP (3.1) by separation of variables, we must solve the *associated Sturm–Liouville (SL) eigenvalue problem (EVP)*:

$$\begin{cases} -\dfrac{\mathrm{d}^6 \psi}{\mathrm{d}x^6} = \lambda^6 \psi, & x \in (-1,1), & \text{(3.2a)} \\ \left.\dfrac{\mathrm{d}\psi}{\mathrm{d}x}\right|_{x=\pm 1} = \left.\dfrac{\mathrm{d}^2 \psi}{\mathrm{d}x^2}\right|_{x=\pm 1} = \left.\dfrac{\mathrm{d}^5 \psi}{\mathrm{d}x^5}\right|_{x=\pm 1} = 0. & & \text{(3.2b)} \end{cases}$$

Although SL theory was developed for second-order problems [25], it is customary in the literature to also refer to higher-order self-adjoint EVPs as "SL EVPs" [26, 27].

As shown in [15], SL EVP (3.2) has a countable set of solutions $\{\psi_m(x)\}_{m=1,2,\ldots}^{\infty}$, which can be split into even ("cosine") $\{\psi_m^c(x)\}_{m=1,2,\ldots}^{\infty}$ and odd ("sine") $\{\psi_m^s(x)\}_{m=1,2,\ldots}^{\infty}$ subsets:

$$\begin{aligned} \psi_m^c(x) = c_m^c \Bigg\{ & \frac{4\sin\lambda_m^c}{\cos\lambda_m^c - \cosh(\sqrt{3}\,\lambda_m^c)} \Bigg[-\cos\left(\frac{\lambda_m^c}{2}\right)\sinh\left(\frac{\sqrt{3}\,\lambda_m^c}{2}\right)\sin\left(\frac{\lambda_m^c}{2}x\right)\sinh\left(\frac{\sqrt{3}\,\lambda_m^c}{2}x\right) \\ & + \sin\left(\frac{\lambda_m^c}{2}\right)\cosh\left(\frac{\sqrt{3}\,\lambda_m^c}{2}\right)\cos\left(\frac{\lambda_m^c}{2}x\right)\cosh\left(\frac{\sqrt{3}\,\lambda_m^c}{2}x\right)\Bigg] + \cos(\lambda_m^c x)\Bigg\}, \end{aligned} \tag{3.3a}$$

$$\begin{aligned} \psi_m^s(x) = c_m^s \Bigg\{ & \frac{4\cos\lambda_m^s}{\cos\lambda_m^s + \cosh(\sqrt{3}\,\lambda_m^s)} \Bigg[-\cos\left(\frac{\lambda_m^s}{2}\right)\cosh\left(\frac{\sqrt{3}\,\lambda_m^s}{2}\right)\sin\left(\frac{\lambda_m^s}{2}x\right)\cosh\left(\frac{\sqrt{3}\,\lambda_m^s}{2}x\right) \\ & + \sin\left(\frac{\lambda_m^s}{2}\right)\sinh\left(\frac{\sqrt{3}\,\lambda_m^s}{2}\right)\cos\left(\frac{\lambda_m^s}{2}x\right)\sinh\left(\frac{\sqrt{3}\,\lambda_m^s}{2}x\right)\Bigg] + \sin(\lambda_m^s x)\Bigg\}, \end{aligned} \tag{3.3b}$$

where the lengthy expressions for the normalization coefficients c_m^c and c_m^s are given in [15].

The eigenvalues λ_m^c correspond to the ψ_m^c and are the solutions of the transcendental equation (3.4a) whereas the λ_m^s correspond to the ψ_m^s and are the solutions of (3.4b):

$$\text{even}: \quad \cos(2\lambda_m^c) + \sqrt{3}\sin\lambda_m^c \sinh(\sqrt{3}\,\lambda_m^c) - \cos\lambda_m^c \cosh(\sqrt{3}\,\lambda_m^c) = 0\,, \tag{3.4a}$$

$$\text{odd}: \quad \sin(2\lambda_m^s) + \sqrt{3}\cos\lambda_m^s \sinh(\sqrt{3}\,\lambda_m^s) + \sin\lambda_m^s \cosh(\sqrt{3}\,\lambda_m^s) = 0\,. \tag{3.4b}$$

Remark 3.1. $\psi_0^c(x) = 1$ satisfies the EVP (3.2) with $\lambda_0 = 0$.

The two sets of solutions ψ_m^c and ψ_m^s of the SL EVP (3.2) given by (3.3) and supplemented by $\psi_0^c = 1$ form a *complete orthonormal* (CON) set of functions on $[-1, 1]$. Thus, given any function $u(x) \in L^2[-1, 1]$, we can write its spectral expansion in this CON basis as

$$u(x) = u_0^c \psi_0^c(x) + \sum_{m=1}^{\infty} u_m^c \psi_m^c(x) + u_m^s \psi_m^s(x), \tag{3.5a}$$

$$u_0^c = \frac{1}{2} \int_{-1}^{1} u(x)\, \mathrm{d}x, \tag{3.5b}$$

$$u_m^c = \int_{-1}^{1} u(x) \psi_m^c(x)\, \mathrm{d}x, \tag{3.5c}$$

$$u_m^s = \int_{-1}^{1} u(x) \psi_m^s(x)\, \mathrm{d}x, \tag{3.5d}$$

where the series (3.5a) converges to $u(x)$ in the mean. For a sketch of the proof, see [15] and the references therein.

4. Solution method (separation of variables)

In this work, we restrict ourselves to initial conditions that are even in space, namely $u^0(x) = u^0(-x)$ on $[-1, 1]$. It is easy to show from (3.1) that it follows that the solution is also even, $u(x, t) = u(-x, t)\ \forall t > 0$.

We solve PDE (3.1a) using an eigenfunction expansion based on sixth-order even eigenfunctions (3.3). Specifically, we write the sought function as $u(x, t) = X(x)T(t)$. Substituting the latter into PDE (3.1a) leads to

$$\frac{T'(t)}{T(t)} = \frac{X^{(6)}(x)}{X(x)} = -\lambda^6, \tag{4.1}$$

where λ must be a constant.

We observe that $X^{(6)}(x) = -\lambda^6 X(x)$ is precisely (3.2a). Subject to the BCs (3.1b), we have shown that it is solved by the even eigenfunctions ψ_m^c corresponding to λ_m^c, i.e., $X(x) = \psi_m^c(x)$ and $\lambda = \lambda_m^c$, $m = 0, 1, 2, \ldots$. Therefore, the general solution is of the form

$$X(x) = \sum_{m=0}^{\infty} u_m \psi_m^c(x), \tag{4.2}$$

where the coefficients $\{u_m\}_{m=0}^{\infty}$ are to be determined. Meanwhile, the IVP $T'(t) = -\lambda^6 T(t)$, $T(0) = T_0$ has solution

$$T(t) = T_0 \mathrm{e}^{-(\lambda_m^c)^6 t}. \tag{4.3}$$

Combining (4.2) and (4.3), using the initial condition $u(x, 0) = u^0(x)$ and recalling remark 3.1, we obtain

$$u(x, t) = u_0^0 \psi_0^c(x) + \sum_{m=1}^{\infty} \mathrm{e}^{-(\lambda_m^c)^6 t} u_m^0 \psi_m^c(x), \tag{4.4a}$$

where $\{u_m^0\}_{m=0}^{\infty}$ are the spectral expansion coefficients of the (even) initial condition $u^0(x)$. From (3.5), we know these coefficients can be obtained by calculating the integrals

$$u_0^0 = \frac{1}{2} \int_{-1}^{1} u^0(x)\, \mathrm{d}x, \tag{4.4b}$$

$$u_m^0 = \int_{-1}^{1} u^0(x) \psi_m^c(x)\, \mathrm{d}x, \qquad m = 1, 2, \ldots, \tag{4.4c}$$

which can be done *exactly* for certain functions $u^0(x)$. When evaluating solutions to specific problems, the infinite sum (4.4a) is truncated at some upper limit $m = M$.

Remark 4.1. The eigenfunctions $\{\psi_m^c(x)\}_{m=0,1,2,\ldots}$ intrinsically satisfy the BCs (3.1b). This guarantees that the solution, as given by (4.4), will also satisfy the BCs (3.1b).

5. Spreading and leveling of finite thin films with elastic interfaces

5.1. Two point loads

Consider IBVP (3.1) with the initial condition

$$u(x,0) = u^0(x) = \frac{1}{2}\Big[\delta(x-\tfrac{1}{2}) + \delta(x+\tfrac{1}{2})\Big], \qquad x \in (-1,1), \tag{5.1}$$

where $\delta(x)$ is the Dirac delta functional (i.e., the unit impulse) centered at $x = 0$.

The IC (5.1) represents two point loads at an equal distance of 1/2 from the center of the domain. This IC has a total "volume"

$$\int_{-1}^{1} u^0(x)\,\mathrm{d}x = 1. \tag{5.2}$$

Although u represents the deviation from a flat interface (see figure 1), u does not have to decay to 0 as $t \to \infty$, since we have free BCs at $x = \pm 1$ that allow for steady states $u(x, t \to \infty) = const. \neq 0$. For an initial perturbation that maintains $u = 0$ at $x = \pm 1$, but is nonvanishing on $(-1, 1)$, some "volume" is added according to (5.2).

Employing well-known properties of the Dirac delta functional (see, e.g., [28]), from (4.4b), (4.4c), and (5.1) we find:

$$u_0^0 = \frac{1}{2}, \tag{5.3a}$$

$$u_m^0 = \frac{1}{2}\Big[\psi_m^c(\tfrac{1}{2}) + \psi_m^c(-\tfrac{1}{2})\Big], \qquad m = 1, 2, \ldots . \tag{5.3b}$$

The spectral expansion of IC (5.1) is shown in figure 2. The strong Gibbs effects observed are expected since (5.1) is not only discontinuous at $x = \pm 1/2$, but is not even a "proper function". The question of whether or not the Gibbs effects in the series expansion affect the accuracy of the spectral solution is addressed in section 5.2.

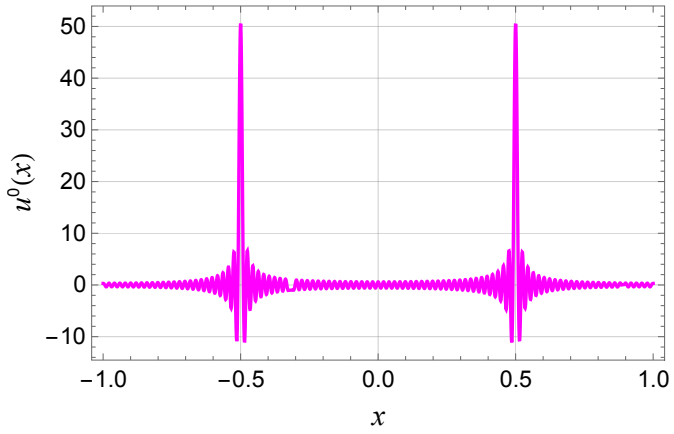

Figure 2. Profile of the spectral representation, which follows from (3.5), of the IC (5.1). The series is truncated at $m = M = 100$ (i.e., 101 terms). Strong Gibbs effects are observed, especially near the discontinuities at $x = \pm 1/2$.

Figure 3 depicts selected snapshots of the solution of this IBVP. Figure 3(a) shows the evolution of the initial disturbance (5.1) from early to intermediate times, whilst figure 3(b) shows how it evolves from

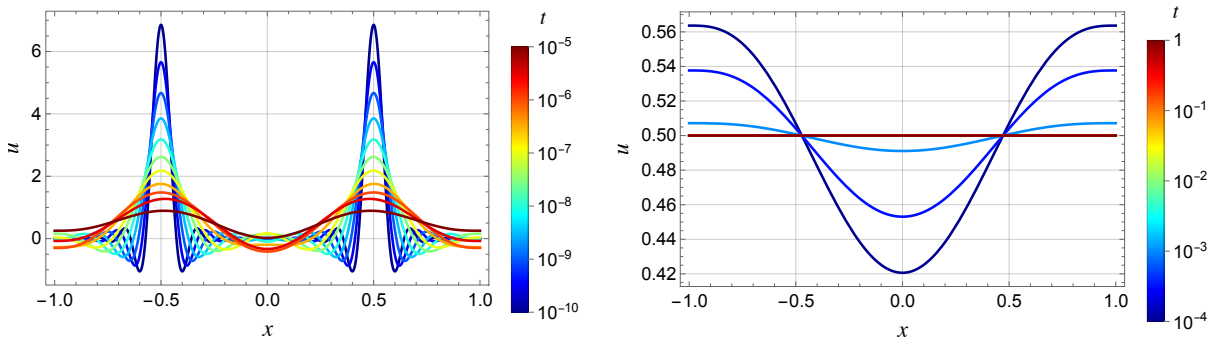

Figure 3. Solution snapshots for IBVP (3.1) subject to IC (5.1). An eigenfunction expansion (4.4a) with 101 terms is used (i.e., truncated at $m = M = 100$). (a) Spreading of the initial disturbance (early to intermediate times). (b) Leveling of the initial disturbance (intermediate to large times). The color scheme represents time on a logarithmic scale, according to each color bar.

intermediate to large times. Of course, the definition of "early" and "late" is not quantitative. Rather, the classification is based on the dynamics observed, which we now analyze.

From figure 3(a), we observe that the point loads create smooth blisters, which spread horizontally. Their amplitudes decay with time. On the other hand, from figure 3(b), it is evident that for $t \geq 10^{-4}$, the solution has spread to the boundaries, with the two blisters coalescing into a profile that exhibits a single local minimum at $x = 0$. The film is now leveling. For $t \geq 10^{-2}$, the solution profile is essentially flat. Importantly, this flat profile has a "volume" equal to one, which is exactly equal to the "volume" (5.2) of the initial condition. This shows that our solution method preserves the steady state.

An important feature of the solution is the *bridge*, namely the point where the two blisters make "contact", following the terminology of Sæter et al. [16]. Here, this point is $x = 0$. Therefore, the bridge height is represented by $u(0, t)$, which is easily formed by evaluating the obtained spectral solution (4.4a) at $x = 0$. Studying the time evolution of the bridge height provides information on how the two blisters "interact". The bridge height $u(0, t)$ is plotted as a function of time in figure 4. Observing figure 4(a), we see that for very early times, $u(0, t)$ oscillates rapidly. However, these oscillations are between relatively small values, namely $-0.017 \leq u(0, t) \leq 0.007$. Concentrating on early to intermediate times in figure 4(b), the bridge initially rises to a maximum value and then decreases, dropping below $u = 0$ and eventually plateauing at a negative lower bound. The maximum and minimum values of $u(0, t)$ over this time range have absolute values that are substantially larger compared to their counterparts in figure 4(a).

A completely different picture is painted by figures 4(c) and 4(d) for $t > 10^{-5}$. Here, later times are presented using a linear abscissa scale in figure 4(c) and a logarithmic abscissa scale in figure 4(d). The length of the time interval here is orders of magnitude larger compared to figures 4(a) and 4(b). The bridge height increases, reaching the equilibrium value $u = 1/2$ at $t \approx 0.015$. Furthermore, figure 4(d) reveals three different regimes according to the rate of increase of $u(0, t)$ with t. These regimes occur over three different time intervals and correspond to different (positive) slopes of the graph of $u(0, t)$ vs t. First, we observe a region of rapid increase, then a region of intermediate positive slope, and finally, a region of almost zero slope corresponding to the equilibration to the final (flat) state.

Now, we quantitatively investigate the asymptotic behavior of the bridge height (as a function of time) for intermediate to large times. Using the obtained solution for the bridge height, $n = 21$ data points $\big(t_i, (u(0, t_i)\big)$, $i = 1, 2, \ldots, n$ were selected for times $t_i \in [10^{-5}, 10^{-1}]$ and fitted to a general exponential function with the aid of MATHEMATICA's [29] `NonlinearModelFit` routine. The results are presented using a linear abscissa scale in figure 5(a) and on a logarithmic abscissa scale in figure 5(b). The best-fit curve was found to be $u(0, t) \simeq \frac{1}{2} - 0.101127\, \mathrm{e}^{-(\lambda_1^c)^6 t} - 1.019245\, \mathrm{e}^{-(\lambda_2^c)^6 t}$, where $\lambda_1^c \approx 3.66606496814$ and

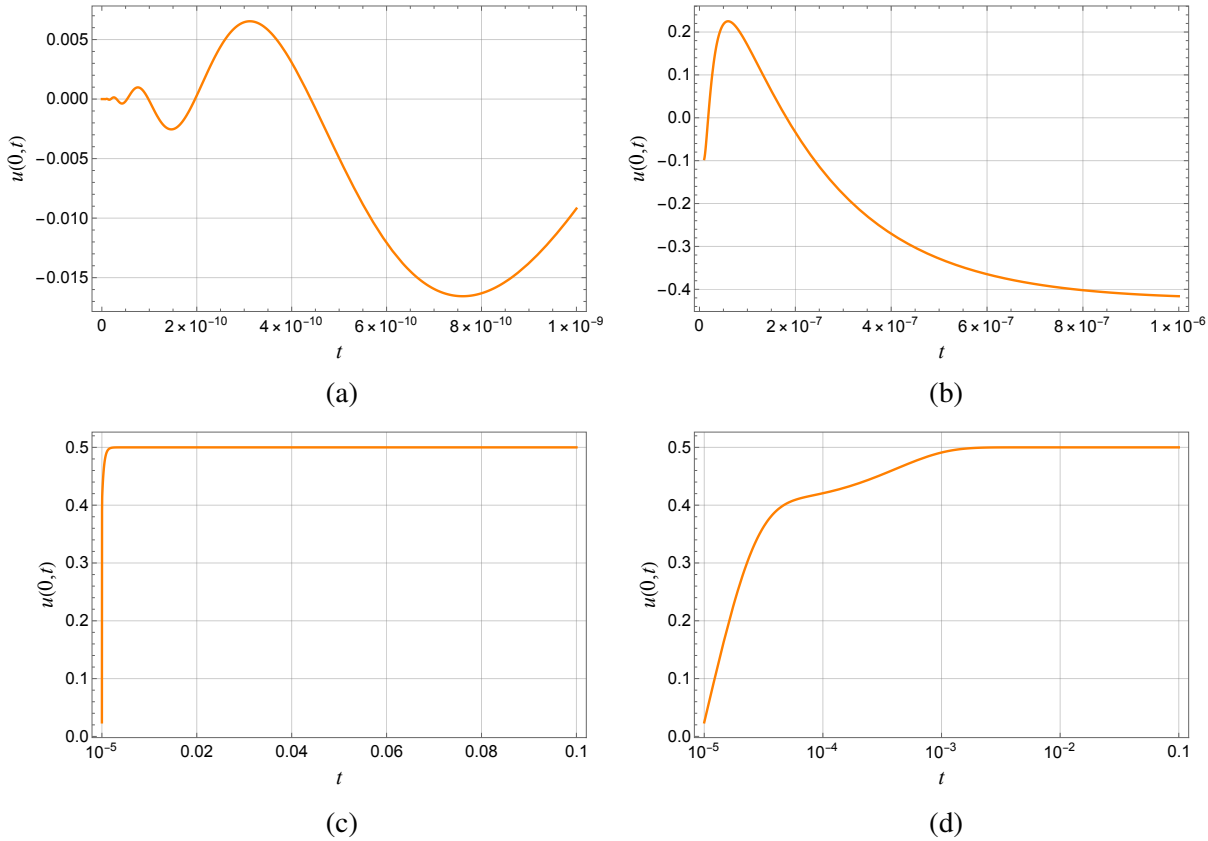

Figure 4. Evolution of the bridge height $u(0,t)$ for IBVP (3.1) subject to IC (5.1) as a function of time: (a) Early times. (b) Intermediate times. (c) Late times. (d) Late times on a log-linear scale.

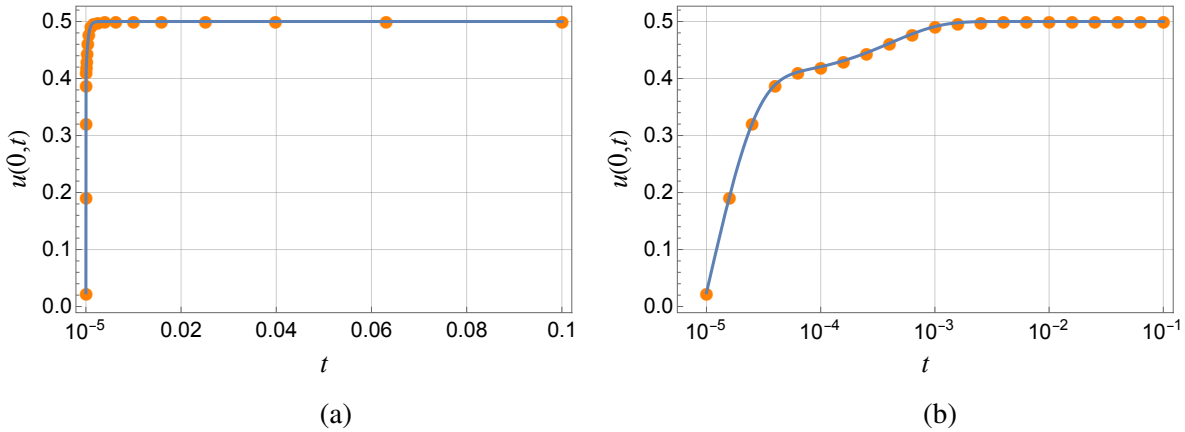

Figure 5. Asymptotic behavior of the bridge height $u(0,t)$ for IBVP (3.1) subject to IC (5.1) for intermediate to large times on (a) linear scale and (b) log-linear scale. Symbols: computed bridge height $u(0,t)$ at the sampling points. Solid: best-fit curve $u(0,t) \simeq \frac{1}{2} - 0.101127\, \mathrm{e}^{-(\lambda_1^c)^6 t} - 1.019245\, \mathrm{e}^{-(\lambda_2^c)^6 t}$.

$\lambda_2^c \approx 6.80678029161$ are the first two nontrivial even eigenvalues of SL EVP (3.2) [15]. Interestingly, this exponential asymptotic behavior of the bridge is similar to what was reported in [16], despite the differences in the two problems. Sæter et al. [16] found the exponential behavior in a *nonlinear* version of the problem on an unconfined domain by seeking a self-similar solution. Here, unlike in [16], the

exponential decay is a direct consequence of solving a linear first-order-in-time PDE (3.1a).

Next, we consider the evolution of the peaks of the blisters, namely $u(\pm 1/2, t)$, as functions of time. The points $x = \pm 1/2$ are the coordinates of the centers of the Dirac deltas (point loads), which appear in IC (5.1). Due to the symmetry of the problem (see also figure 3), $u(-1/2, t) = u(1/2, t)$, $\forall t \geq 0$. Therefore, it suffices to consider only $u(1/2, t)$. Now, using the same sampling points $\{t_i\}_{i=1}^{21}$ as those selected for fitting the bridge height, as well as the same computational routine, we find the best-fit curve $u(1/2, t) \simeq \frac{1}{2} + 1.066850\, \mathrm{e}^{-(\lambda_2^c)^6 t}$. Therefore, in contrast to our findings for the bridge height, the eigenmode corresponding to λ_1^c does not participate in the dynamics of the blister height decay. The results for $t \geq 10^{-5}$ are presented using a linear abscissa scale in figure 6(a) and using a logarithmic abscissa scale in figure 6(b). Indeed, we observe that the decay of $u(1/2, t)$ has only two distinct regimes: (i) a region of rapid decrease for $10^{-5} \leq t \leq 10^{-4}$ and (ii) a region of almost zero slope corresponding to the equilibration to the final (flat) state ($u = 1/2$) for $t > 10^{-4}$.

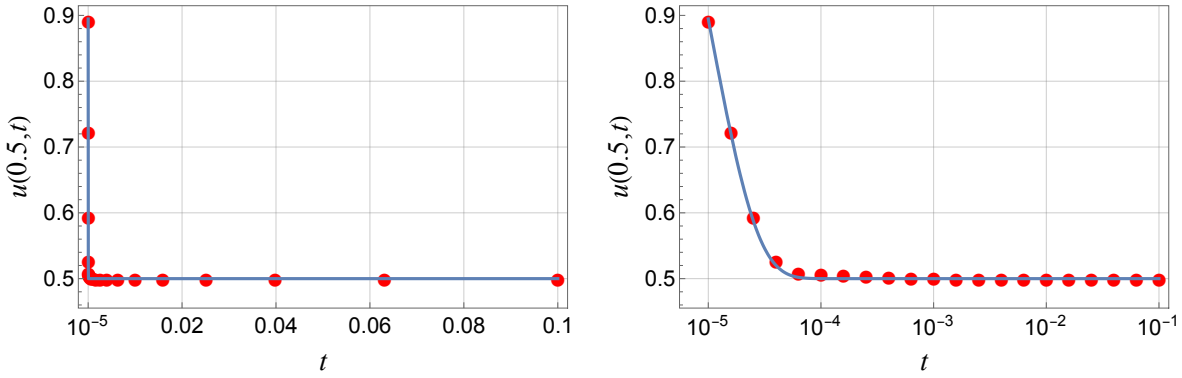

Figure 6. Asymptotic behavior of the blister heights $u(1/2, t)$ for IBVP (3.1) subject to IC (5.1) for intermediate to large times on (a) linear scale and (b) log-linear scale. Symbols: computed bridge height $u(1/2, t)$ at the sampling points. Solid: best-fit curve $u(1/2, t) \simeq \frac{1}{2} + 1.066850\, \mathrm{e}^{-(\lambda_2^c)^6 t}$.

5.2. Two smooth bumps

Now, consider IBVP (3.1) subject to the (continuous) piecewise polynomial initial condition

$$u_0(x) = \begin{cases} \frac{15}{8}\left[1 - \frac{(x+\frac{1}{2})^2}{(\frac{1}{4})^2}\right]^2 & \text{if } -\frac{3}{4} \leq x \leq -\frac{1}{4}, \\ \frac{15}{8}\left[1 - \frac{(x-\frac{1}{2})^2}{(\frac{1}{4})^2}\right]^2 & \text{if } \frac{1}{4} \leq x \leq \frac{3}{4}, \\ 0 & \text{otherwise}. \end{cases} \tag{5.4}$$

This IC (5.4) is an adaptation of the function used by Sæter et al. [16] to model the two elastic blisters of their experimental study. In the present context, the shape function has been reduced to a function of a single spatial variable, x, and normalized to have unit "volume" on $x \in [-1, 1]$. It is important to note that (5.4) is a smooth and even function of x, exhibiting no discontinuities and satisfying BCs (3.2b).

The eigenfunction expansion of IC (5.4) is truncated at $M = 100$ and is compared to the function it approximates in figure 7(a). As we have already noted, this IC is a smooth function satisfying the same BCs as the ψ_m^c eigenfunctions. Hence, there is an excellent agreement between (5.4) and its spectral expansion (the profiles in the figure are essentially indistinguishable), which should be expected. In figure 7(b), we further present the spatial variation of the absolute difference between the IC and its

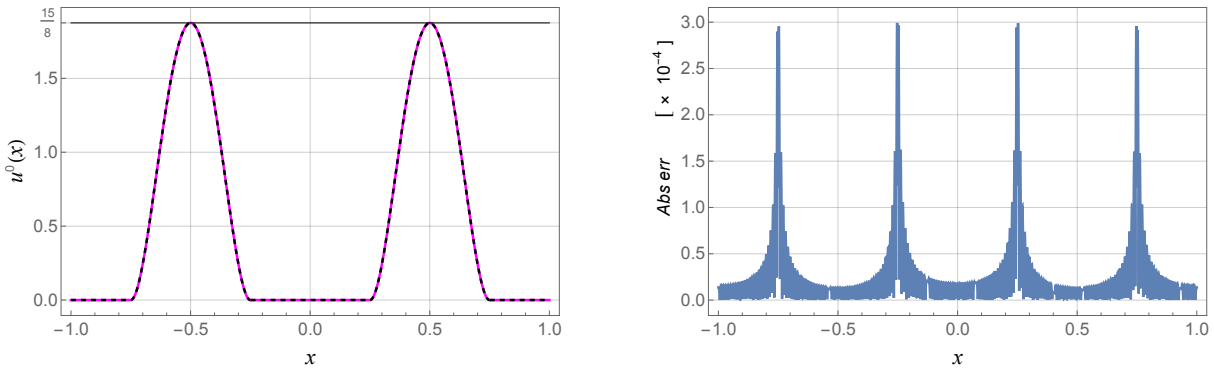

Figure 7. (a) Solid: profile of the IC as given by (5.4). Dashed: its spectral approximation, which follows from (3.5), truncated at $m = M = 100$. (b) The absolute error between $u^0(x)$ and its spectral expansion.

spectral representation. We observe that the maximum absolute error is $< 3 \times 10^{-4}$ and that there is no visible Gibbs effects.

As before, the solution $u(x,t)$ of IBVP (3.1) subject to IC (5.4) can be written as (4.4a), however evaluating the expansion coefficients, via (4.4b) and (4.4c), based on the IC (5.4), is more tedious. Thus, the lengthy expressions for the coefficients $\{u_m^0\}_{m=0,1,2,\ldots}$ are given by (A.1) in the Appendix.

In figure 8, we present snapshots of the eigenfunction solution of IBVP (3.1) subject to IC (5.4). From figure 8(a) (early to intermediate times), we see that the blisters centered at $x = \pm 1/2$ decrease in height, with the solution spreading out. In figure 8(b) (intermediate to later times), the blisters have already coalesced into a single smooth bump centered at $x = 0$ by $t \approx 10^{-4}$. As time increases, the (absolute) height of this bump, namely $|u(0,t)|$, reduces, with the solution essentially reaching the flat equilibrium state ($u = 1/2$) at $t \approx 10^{-2}$. Once again, the "volume" of the equilibrium state is conserved. The behavior exhibited here is *qualitatively* (but not quantitatively) similar to that shown in figure 3, highlighting the universal aspects of spreading and leveling of finite thin films with elastic interfaces.

The evolution of the bridge height $u(0,t)$ with time for IBVP (3.1) subject to IC (5.4) is illustrated in figure 9. The time intervals and scales used in figures 9(a)-(d) are the same as their counterparts in figures 4(a)-(d). Comparing the two figures, we observe that the bridge heights corresponding to blisters emerging from the two different ICs exhibit similar behavior. The same remarks and observations made

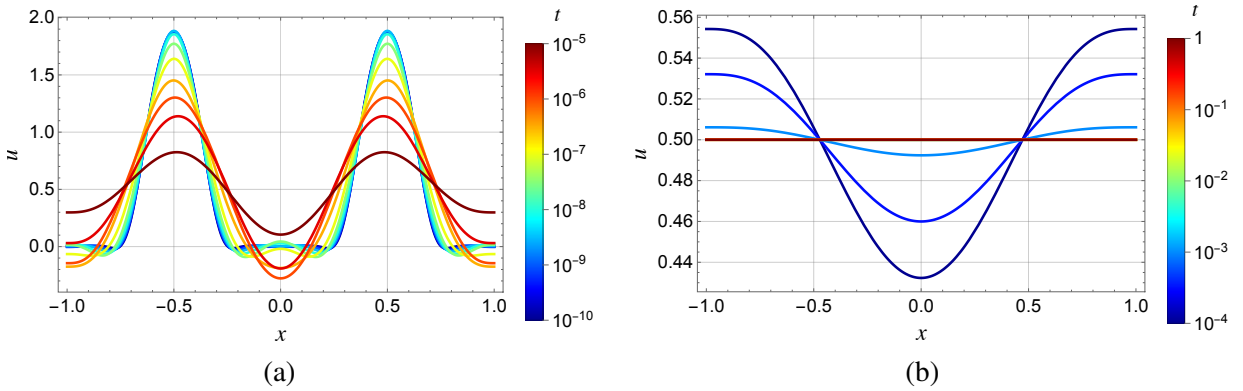

Figure 8. Solution snapshots for IBVP (3.1) subject to IC (5.4). (a) spreading of the initial disturbance (early to intermediate times). (b) leveling of the initial disturbance (intermediate to large times). Notice the similarity of the leveling curves between the two different ICs.

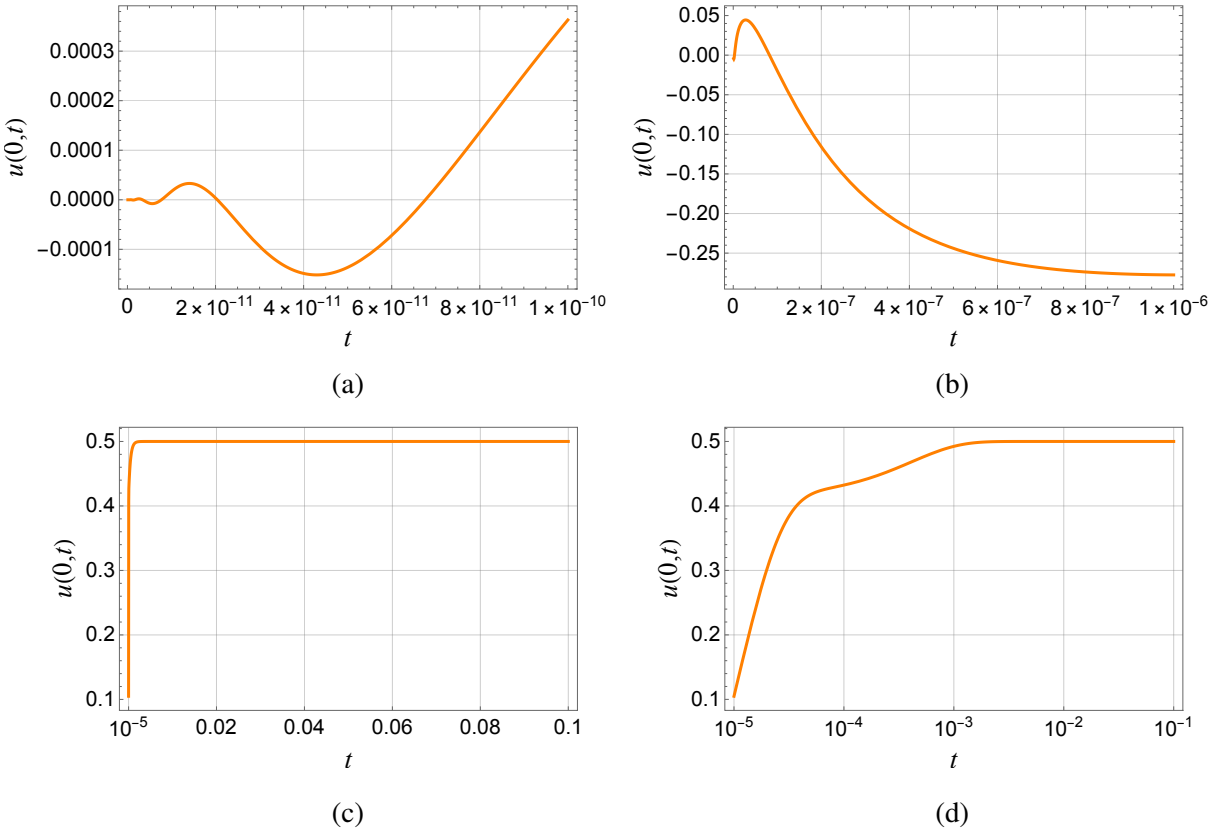

Figure 9. Evolution of the bridge height $u(0,t)$ of the solution of IBVP (3.1) subject to IC (5.4) as a function of time: (a) Early times. (b) Intermediate times. (c) Late times. (d) Late times on a log-linear scale.

when discussing figures 4(a)-(d) in the previous subsection also hold here. Other than the expected quantitative differences, perhaps the only other difference of note is that for very early times, the bridge height in figure 9(a) is slightly less oscillatory compared to that in figure 4(a).

We may, therefore, conclude that the small-amplitude oscillations observed at very early times are not an artifact of the solution method (for instance, a result of the Gibbs effects) but a characteristic of the problem since they are also present when our IC is smooth and has an accurate well-behaved eigenfunction expansion. In addition, *both* figures 9(b),(d) and figures 4(b),(d) show that for the time interval $t \in [2\times10^{-7}, 10^{-6}]$ the bridge height is negative. This means that following some very small (in amplitude) oscillations at very early times and after contact between the two blisters is established, the elastic interface in the vicinity of the point of contact drops below the initial equilibrium film height (the flat state $u = 1/2$) before it eventually rises back to it as $t \to \infty$. These negative values were not observed in [16] since that work concentrated on intermediate to later times, with the computational time being reset to zero once contact was made.

In figure 10, we examine the asymptotic behavior of the bridge height evolving from the two bumps IC (5.4) following the same method as that of figure 5 for the two point loads IC. Once again, we find that the best-fit function (obtained from MATHEMATICA) is exponential and that it involves the first two nontrivial even eigenvalues, namely $u(0,t) \simeq \frac{1}{2} - 0.086219\,\mathrm{e}^{-(\lambda_1^c)^6 t} - 0.840805\,\mathrm{e}^{-(\lambda_2^c)^6 t}$. The results are presented using a linear abscissa scale in figure 10 (a) and using a logarithmic abscissa scale in figure 10(b).

Finally, in figure 11, we study the time-evolution of the blister heights $u(1/2,t)$ in the same way as in

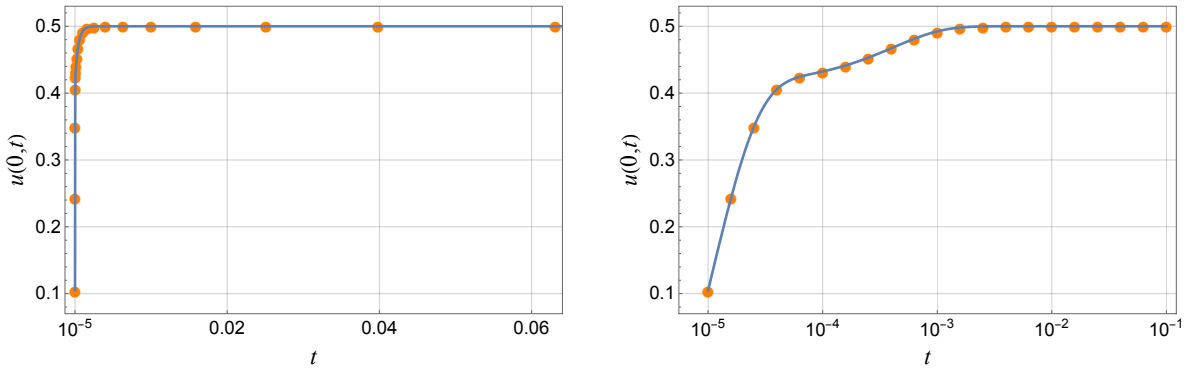

(a) (b)

Figure 10. Asymptotic behavior of the bridge heighfor IBVP (3.1) subject to IC (5.4) for intermediate to large times on (a) linear scale and (b) log-linear scale. Symbols: computed bridge height $u(0,t)$. Solid: best-fit curve $u(0,t) \simeq \frac{1}{2} - 0.086219\,\mathrm{e}^{-(\lambda_1^c)^6 t} - 0.840805\,\mathrm{e}^{-(\lambda_2^c)^6 t}$.

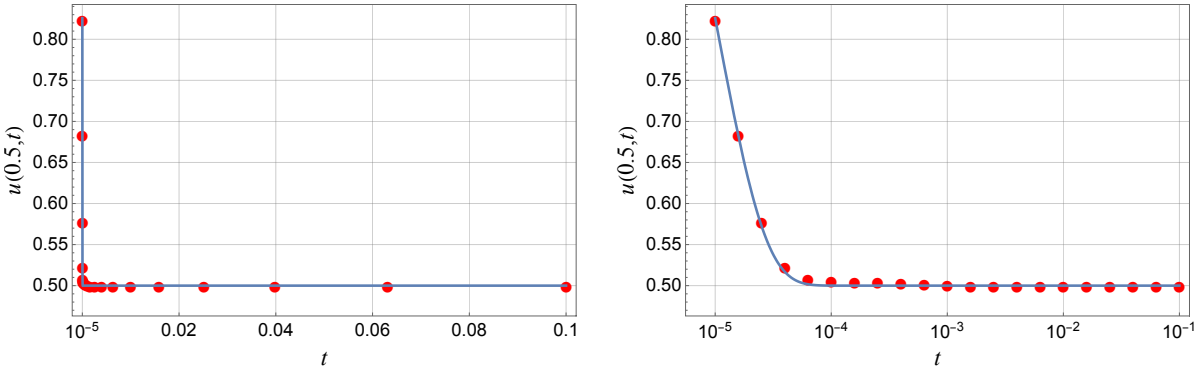

(a) (b)

Figure 11. Asymptotic behavior of the bumps' heights $u(\pm 1/2, t)$ for IBVP (3.1) subject to IC (5.4) for intermediate to large times on a (a) linear scale and (b) log-linear scale. Symbols: computed bridge height $u(1/2,t)$. Solid: best-fit curve $u(1/2,t) \simeq \frac{1}{2} + 0.880922\,\mathrm{e}^{-(\lambda_2^c)^6 t}$.

section 5.1. Once again, the best-fit function is exponential, involving only the zeroth and second, but not first, eigenvalues of the problem. The best-fit curve is now $u(1/2,t) \simeq \frac{1}{2} + 0.880922\,\mathrm{e}^{-(\lambda_2^c)^6 t}$. In addition, we observe the same two regimes of decay of $u(1/2,t)$, as we previously did in figure 6, indicative of (i) spreading and (ii) leveling of the film.

6. Conclusion

We studied the linearized dynamics of spreading and leveling of thin films with elastic interfaces laterally confined in finite-length troughs in the absence of gravity. The governing sixth-order IBVP was solved using separation of variables and the even functions of the complete orthonormal (CON) basis previously developed in [15].

Two exemplar problems with even ICs were solved to demonstrate how initial perturbations of the film height lead to the development, spreading, and leveling of blisters on the film. In the first case, the non-smooth IC was the semi-sum of two translated delta "functions" equidistant from the origin, and in the second, the smooth IC was the sum of two quartics with finite support and vertices equidistant from

the origin. In both cases, the coefficients of the spectral expansions were found exactly (analytically).

We observed that the leveling of the two different initial disturbances considered was qualitatively the same, suggesting that any Gibbs' effects in the expansion of non-smooth ICs do not affect the dynamics. Our observations also highlight the universal aspects of spreading and leveling under a linear sixth-order equation of "parabolic" type. We found that in both cases, the time-dependence of the bridge height for intermediate to large times is *exponential* and determined by the first two non-trivial modes' eigenvalues, λ_1^c and λ_2^c, of the problem. In both cases, the time dependence of the blisters' heights was also found to be exponential for intermediate to large times. However, their evolution is set by *only* λ_2^c.

Acknowledgments
ICC would like to acknowledge the US National Science Foundation, which supports his research on interfacial dynamics under grant CMMI-2029540.

Appendix
The expressions for the coefficients u_m^0 used in the expansion of the initial condition (5.4) into even eigenfunctions ψ_m^c from (3.3a) are given by:

$$u_0^0 = 1, \tag{A.1a}$$

$$u_m^0 = \frac{n_m^c}{\sqrt{d_m^c}}, \qquad \text{where} \tag{A.1b}$$

$$\begin{aligned} n_m^c = 960\Big\{ & 2\cos\tfrac{\lambda_m^c}{2}\Big[12\lambda_m^c\cos\tfrac{\lambda_m^c}{4}\cosh\sqrt{3}\lambda_m^c + (-48+(\lambda_m^c)^2)(-\cos\lambda_m^c+\cosh\sqrt{3}\lambda_m^c)\sin\tfrac{\lambda_m^c}{4}\Big] \\ & - 6\lambda_m^c\cos\lambda_m^c\csc\tfrac{\lambda_m^c}{4}\sin\lambda_m^c \\ & +2(\cos\tfrac{\lambda_m^c}{2}+\cosh\tfrac{\sqrt{3}}{2}\lambda_m^c)\sin\lambda_m^c\times\Big[-2(24+(\lambda_m^c)^2)\cos\tfrac{3}{8}\lambda_m^c\cosh\tfrac{\sqrt{3}}{8}\lambda_m^c + 48\sqrt{3}\sin\tfrac{3}{8}\lambda_m^c\sinh\tfrac{\sqrt{3}}{8}\lambda_m^c \\ & + 12\lambda_m^c\Big(\cosh\tfrac{\sqrt{3}}{8}\lambda_m^c\sin\tfrac{3}{8}\lambda_m^c - \sqrt{3}\sinh\tfrac{\sqrt{3}}{8}\lambda_m^c\cos\tfrac{3}{8}\lambda_m^c\Big) \\ & - 12\sqrt{3}(\lambda_m^c\cos\tfrac{\lambda_m^c}{8}+4\sin\tfrac{\lambda_m^c}{8})\sinh\tfrac{3\sqrt{3}}{8}\lambda_m^c + 2\cosh\tfrac{3\sqrt{3}}{8}\lambda_m^c\Big((24+(\lambda_m^c)^2)\cos\tfrac{\lambda_m^c}{8}\Big]\Big\}, \end{aligned} \tag{A.1c}$$

$$\begin{aligned} d_m^c = (\lambda_m^c)^9\Big\{ & (-6\lambda_m^c(-2+\cos 2\lambda_m^c)+2\lambda_m^c\cosh 2\sqrt{3}\lambda_m^c + 2\cosh^2\sqrt{3}\lambda_m^c\sin 2\lambda_m^c + \sin 4\lambda_m^c \\ & + \cosh\sqrt{3}\lambda_m^c\Big(4\lambda_m^c(-3\cos\lambda_m^c+\cos 3\lambda_m^c)+\sin\lambda_m^c - 3\sin 3\lambda_m^c\Big) \\ & + 4\sqrt{3}(\cos\lambda_m^c-\cosh\sqrt{3}\lambda_m^c)\sin^2\lambda_m^c\sinh\sqrt{3}\lambda_m^c)\Big\}, \qquad m=1,2,\ldots. \end{aligned} \tag{A.1d}$$

References

[1] Hosoi A E and Mahadevan L 2004 *Phys. Rev. Lett.* **93** 137802
[2] Peng G G and Lister J R 2020 *J. Fluid Mech.* **905** A30
[3] Michaut C 2011 *J. Geophys. Res.: Solid Earth* **116** B05205
[4] Bunger A P and Cruden A R 2011 *J. Geophys. Res.: Solid Earth* **116** B02203
[5] Bunger A P and Cruden A R 2011 *J. Geophys. Res.: Solid Earth* **116** B08211
[6] Kodio O, Griffiths I M and Vella D 2017 *Phys. Rev. Fluids* **2** 014202 (*Preprint* arXiv:1609.04598)
[7] Pedersen C, Niven J F, Salez T, Dalnoki-Veress K and Carlson A 2019 *Phys. Rev. Fluids* **4** 124003 (*Preprint* arXiv:1902.10470)
[8] Huang R and Suo Z 2002 *J. Appl. Phys.* **91** 1135–1142
[9] King J R 1989 *SIAM. J. Appl. Math.* **49** 1064–1080
[10] Boyko E, Eshel R, Gommed K, Gat A D and Bercovici M 2019 *J. Fluid Mech.* **862** 732–752 (*Preprint* arXiv:1703.06820)
[11] Tulchinsky A and Gat A D 2016 *J. Fluid Mech.* **800** 517–530 (*Preprint* arXiv:1512.00730)
[12] Richards J A, Hodgson D J M, O'Neill R E, DeRosa M E and Poon W C K 2024 *Proc. Natl Acad. Sci. USA* **121** e2317832121 (*Preprint* arXiv:2311.08280)
[13] Carlson A and Mahadevan L 2016 *Phys. Fluids* **28** 011702 (*Preprint* arXiv:1507.03912)
[14] Poulain S, Carlson A, Mandre S and Mahadevan L 2022 *J. Fluid Mech.* **947** A16
[15] Papanicolaou N C and Christov I C 2023 *J. Phys.: Conf. Ser.* **2675** 012016 (*Preprint* arXiv:2308.00673)
[16] Sæter T, Pedersen C, Snoeijer J H, Salez T and Carlson A 2024 *Phys. Rev. Lett.* **132** 074001 (*Preprint* arXiv:2308.01774)
[17] Longley J E, Mahadevan L and Chaudhury M K 2013 *EPL* **104** 46002 (*Preprint* arXiv:1402.0262)
[18] Pedersen C, Salez T and Carlson A 2021 *Proc. R. Soc. A* **477** 20210354 (*Preprint* arXiv:2011.10297)
[19] Papanicolaou N C and Christov I C 2024 *submitted* (*Preprint* arXiv:2402.18740)
[20] Oron A, Davis S H and Bankoff S G 1997 *Rev. Mod. Phys.* **69** 931–980
[21] Craster R V and Matar O K 2009 *Rev. Mod. Phys.* **81** 1131–1198
[22] Leal L G 2007 *Advanced Transport Phenomena: Fluid Mechanics and Convective Transport Processes* (*Cambridge Series in Chemical Engineering* vol 7) (New York, NY: Cambridge University Press)
[23] Hewitt I J, Balmforth N J and De Bruyn J R 2015 *Eur. J. Appl. Math.* **26** 1–31
[24] Elbaz S B and Gat A D 2014 *J. Fluid Mech.* **758** 221–237
[25] Marchenko V A 2014 *Sturm-Liouville Operators and Applications* Operator Theory: Advances and Applications (Birkhäuser Basel)
[26] Greenberg L and Marletta M 1998 *SIAM J. Numer. Anal.* **35** 2070–2098
[27] Greenberg L and Marletta M 2000 *J. Comput. Appl. Math.* **125** 367–383
[28] *NIST Digital Library of Mathematical Functions*, Release 1.2.1 of 2024-06-15. F. W. J. Olver, A. B. Olde Daalhuis, D. W. Lozier, B. I. Schneider, R. F. Boisvert, C. W. Clark, B. R. Miller, B. V. Saunders, H. S. Cohl, and M. A. McClain, eds. URL `https://dlmf.nist.gov/`
[29] Wolfram Research, Inc 2024 Mathematica, Version 14.0 Champaign, IL URL `https://www.wolfram.com/mathematica`